VI International Conference on Computational Methods in Marine Engineering
MARINE 2015
F. Salvatore, R. Broglia and R. Muscari (Eds)

ANALYSIS OF THE UNSTEADY WAKE OF A FULL BOTTOMED SHIP IN SHALLOW WATER

IVAN SHEVCHUK*, NIKOLAI KORNEV

*Chair of Modeling and Simulation, University of Rostock
Albert-Einstein Str. 2, 18059,
Rostock, Germany
ivan.shevchuk@uni-rostock.de

Key words: Hybrid RANS/LES, shallow water, unsteady wake, vibration

Abstract. The paper is devoted to the analysis of the unsteady hydrodynamic processes taking place in the ship wake under shallow water conditions. The motivation of the research is the determination of the reasons for the rise of strong vibration in the stern of inland cruise ships in the waterways with considerable depth restriction.

As a research tool the hybrid URANS/LES approach of Kornev et al. [1] is selected in order to capture the influence of nonstationary vortical structures on the velocity oscillations in the propeller plane. As it will be shown, URANS method cannot reproduce these flow features.

The flow is studied in a single-phase and in a two-phase formulation. Influence of the free surface, depth Froude number and depth to draft ratio on the wake is analyzed. The adverse pressure gradient in the stern region causes massive separations of the boundary layer. On account of the separations the velocity oscillations in the wake are turned out to be strongly dependent on the under keel clearance.

On the other hand, it is shown, that at high Fr_H the wave pattern can significantly influence the viscous wake and cause the suppression of the velocity oscillations due to the decrease of the water level. Possible effect of the wake unsteadiness on the propeller performance in such circumstances is discussed.

1 INTRODUCTION

One of the effects, which characterizes the ship motion under shallow water conditions is the vibration, arising in the stern. According to Barrass [2] it is one of the common signs that the ship entered the fairway with depth restriction. The reason for this phenomenon as it is described in the mentioned work is the resonance caused by the coincidence of the hull natural frequency with the frequency of flow oscillations.

Particularly this problem can be observed on inland cruise ships. Such vessels often pass through the extreme shallow waters and while passing them the strong vibration

appears in the stern. The passenger cabins in this part of the ship are located right above the engine room, and when the described above resonance occurs, passengers feel themselves uncomfortable. Therefore there is a need for a deeper understanding of the processes taking place in the stern region, in order to provide some recommendations for the shipyards regarding the vibration treatment.

The exciters of ship vibration can be split into two groups: mechanical and hydrodynamical ones [3]. The former group includes main and auxiliary engines, shaft machinery, gearboxes, etc. The main reason of the hydrodynamically excited vibration is the propeller. Its blades rotating in water create pressure pulses on the hull and cause the oscillations of the hull sheeting. Additionally, the nonuniformity of the wake leads to the rise of the periodic oscillations of forces and moments, produced by the propellers. These periodic forces are transmitted through the shafting to the ship structure. One more effect, which can play a significant role for the vibration is the unsteadiness of the wake. In fact, the velocity field in the stern of a ship is not constant in time, it can also oscillate and cause additional unsteady loadings.

Generally speaking, the study of the reasons for vibration should involve both hydromechanical and structural analysis. However, in this particular case, when the vibration occurs because of the depth restriction, it is to expect, that the hydromechanical effects, play a major role. Moreover, FSI simulations for the problem under consideration is a very complicated task. It was therefore decided to analyze the hydrodynamical part of the problem first and clarify, which mechanisms can potentially influence the ship vibration from the fluid side, in particular, how the change of the wake in shallow water influences the propeller. Therefore the structural analysis is left out of the scope of the current research and thus present work deals with the simulation of the unsteady ship wake in shallow water. As an object for the study the generic geometry of the inland cruise vessel is selected.

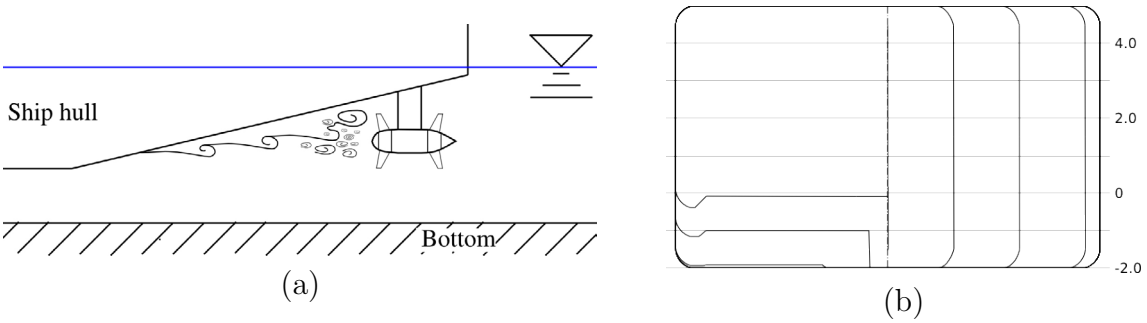

Figure 1: (a) - sketch of the stern flow geometry of an inland cruise vessel ,(b) - body plan of the generic hull form

1.1 Turbulence modeling

The main challenge one faces when solving such a task is the turbulence modeling. The flow configuration in the stern of a studied vessel is similar to that in a diffuser (see Fig. 1, which means that the flow in this region is subject to the adverse pressure gradient and therefore, one could expect that the flow separation occurs which would generate the unsteady vortical structures, passing to the propeller plane and causing the oscillations of forces and moments, produced by the propulsor. Evolution of these vortices, detached from the ship hull has to be resolved in order to account for unsteady effects in the wake.

URANS approach, widely used for industrial applications nowadays, can provide satisfactory results for many tasks like resistance prediction, ship motion in waves, open water propeller tests, etc.[4, 5]. However, when it comes to the unsteady effects, which are not driven by the inflow conditions or motion of the boundaries, URANS tends to damp the inner flow instabilities [6]. Application of URANS method to the case of interest, as it will be shown later, results in a steady solution.

Table 1: Summary of the computed cases

Case label	1PH61	1PH62	2PH61	2PH62	2PH41	2PH42
Fn_H [-]	1.21	1.1	1.21	1.1	0.81	0.74
H/T [-]	1.25	1.5	1.25	1.5	1.25	1.5
$u_\infty\,[ms^{-1}]$	6	6	6	6	4	4
FS	no	no	yes	yes	yes	yes

For the reasons described above some type of scale resolving simulation (SRS) should be applied for the problem. LES, being the most well understood SRS concept, bears practical difficulties in near-wall regions for flows at high Re. The reason for this is that the resolution of 80% of the energy of the near-wall motions requires a number of computational cells, which being scaled with the Reynolds number [7] gets enormous when Re increases. Thus, pure LES is unfeasible for the considered flow.

An alternative approach, which is used in the present work, is the hybrid RANS/LES modeling. Roughly speaking, its strategy is to model the near-wall turbulence with statistical methods and to resolve the turbulent motions remote from the wall explicitly using

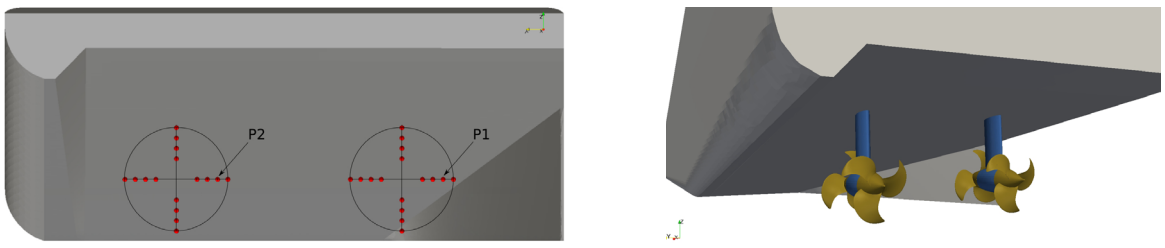

Figure 2: Left: probe points for u_x. Right: The view of the stern geometry with propellers

LES. In the past decade a huge number of different hybrid techniques was developed, for the review the reader is referred to [6, 8].

2 COMPUTATIONAL MODEL

2.1 Hybrid URANS/LES method

In this study the hybrid URANS/LES approach of Kornev et al. [1] is adopted. This hybrid method follows the concept of unified soft-interface modeling (see [6]), where the transport equation

$$\frac{\partial \overline{u}_i}{\partial t} + \frac{\overline{u}_i \overline{u}_j}{\partial x_j} = -\frac{\partial \overline{p}^*}{\partial x_i} + \frac{\partial (\tau^l_{ij} + \tau^t_{ij})}{\partial x_j}, \tag{1}$$

for a hybrid velocity $\overline{u}$ is solved continuously in the whole domain. Here $\overline{p}^* = \overline{p} + \frac{2}{3}k$ is the hybrid modified pressure, τ^l_{ij}, τ^t_{ij} - laminar and turbulent anisotropic stress tensors respectively. The latter are represented by the following formulas:

$$\tau^l_{ij} = 2\,\nu \overline{S}_{ij}$$
$$\tau^t_{ij} = 2\,\nu_{hyb} \overline{S}_{ij}$$

with $\overline{S}_{ij} = \frac{1}{2}(\frac{\partial \overline{u}_i}{\partial x_j} + \frac{\partial \overline{u}_j}{\partial x_i})$ being a strain-rate tensor. The model of viscous incompressible fluid is considered and therefore Eq. (1) is accompanied by the continuity equation:

$$\frac{\partial \overline{u}_i}{\partial x_i} = 0. \tag{2}$$

Computational domain is dynamically decomposed into RANS and LES regions based on the ratio $h = h(\vec{x}, t) = L(\vec{x}, t)/\Delta(\vec{x})$ between the integral length scale L and the characteristic cell size $\Delta = \sqrt{0.5(\Delta^2_{max} + V^{2/3})}$. The difference between the RANS and LES regions is the way how ν_{hyb} field is calculated. Generally, it can be represented as a weighted sum of kinematic turbulent viscosity and subgrid scale viscosity:

$$\nu_{hyb} = \gamma \nu_t + (1 - \gamma)\nu_{sgs}, \tag{3}$$

where $\gamma = \gamma(\vec{x}, t)$ is a blending function, which reads:

$$\gamma = \begin{cases} 0, & h > h_2 \\ 1, & h < h_1 \\ f_\gamma(h), & h_1 \le h \le h_2 \end{cases} \tag{4}$$

$$f_\gamma = \frac{1}{2} + \frac{1}{\pi} \arctan\left(40 \frac{h_1 - h}{(h_2 - h_1)^2} + 10 \frac{h_2 + h_1}{h_2 - h_1}\right)$$

If a cell has $h > h_2$, it is supposed that the resolution is sufficient to resolve the inertial range one obtains the subgrid viscosity, modeled using Lilly's modification of Germano dynamic model [9]:

$$\nu_{sgs} = (C_s\Delta)^2|\overline{S}| \tag{5}$$

Cells, having $h < h_1$ are considered too large, and for them the turbulent kinematic viscosity ν_t is calculated using Menter's $k-\omega$ SST model [10], equations for k, ω are solved in the background. Parameters h_1 and h_2 were chosen as 0.95 and 1.05 respectively.

To estimate the integral length scale L, the Prandl-Kolmogorov formula [11] without a correction factor is used. Recalling, that $\omega = \frac{\epsilon}{k\beta^*}$, one can obtain:

$$L = \frac{k^{3/2}}{\epsilon} = \frac{\sqrt{k}}{\beta^*\omega}, \tag{6}$$

where $\beta^* = 0.09$. This way L is represented in terms of turbulent quantities, used in underlying $k-\omega$ SST model. Hybrid viscosity, obtained in the described manner is also used for the calculation of the production and diffusion terms in k and ω equations. For further details of model formulation the reader is referred to [1, 12].

The approach presented above was implemented in OpenFOAM® library and validated for naval hydrodynamics applications [12].

2.2 Free surface modeling

In the previous subsection a single-phase formulation of the model was presented. However, under shallow water conditions it is also desirable to study the influence of the free surface on the flow in the stern. In the present research it is done by using the volume-of-fluid (VOF) method and particularly its implementation in OpenFOAM-2.3.x (`interFoam` solver). The system of equations of the considered model reads:

$$\frac{\partial\rho\overline{u}_i}{\partial t} + \frac{\partial(\rho\overline{u}_i\overline{u}_j)}{\partial x_j} = -\frac{\partial\overline{p_d^*}}{\partial x_i} + \frac{\partial}{\partial x_j}\left[\mu_{tot}\left(\frac{\partial\overline{u}_i}{\partial x_j} + \frac{\partial\overline{u}_j}{\partial x_i}\right)\right] - g_i x_i\frac{\partial\rho}{\partial x_i} + \sigma\kappa\frac{\partial\alpha}{\partial x_i} \tag{7}$$

$$\frac{\partial\overline{u}_i}{\partial x_i} = 0 \tag{8}$$

$$\frac{\partial\alpha}{\partial t} + \frac{\partial\alpha u_j}{\partial x_j} + \frac{\partial}{\partial x_j}(\alpha(1-\alpha)u_{rj}) = 0 \tag{9}$$

Here α is a volume fraction of water, $\kappa = \nabla\cdot\left(\frac{\nabla\alpha}{|\nabla\alpha|}\right)$ - interface curvature, u_r - interface compression velocity, σ - surface tension, $\mu_{tot} = (\nu_{hyb} + \nu)\rho$ - total dynamic viscosity, $\overline{p_d^*} = \overline{p^*} - \rho g_i x_i$ - dynamic pressure, $\vec{g}$ - gravitational acceleration. The density of a two-phase mixture $\rho = \alpha\rho_{water} + (1-\alpha)\rho_{air}$. Description of the solution procedure for the system (7)-(9) can be found for example in [13].

Hybrid viscosity ν_{hyb} is calculated in the same manner as in a single-phase formulation.

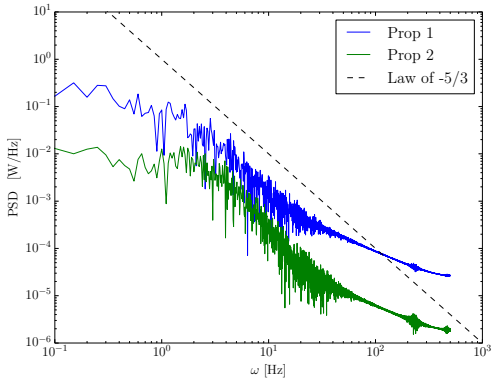

Figure 3: Power spectral density of the velocity fluctuations in the propeller disks at different H/T ratios, 1PH61

	Δu_x^{max}		s	
	P1	P2	P1	P2
1PH61	0.38	0.08	0.84	0.17
1PH62	0.54	0.06	1.11	0.10
2PH61	0.09	0.03	0.21	0.05
2PH62	0.03	0.04	0.04	0.08
2PH41	0.68	0.17	0.99	0.17
2PH42	0.50	0.12	1.01	0.18

Table 2: Maximum and standard deviation of the longitudinal velocity for different cases at points P1 and P2

3 DESCRIPTION OF CONSIDERED CASES

A CAD description of the ship under consideration was unavailable, that is why the generic hull form was used, which had the same dimensions (L_{wl} = 135 m, B=12 m, T=2 m) and similar form. Its body plan and 3D stern geometry with propellers are shown in the Fig. 1, 2. Computations were performed for the bare hull. Since the phenomena to be studied (e.g. boundary layer separation) are dependent on Re and are hardly scalable, it was decided to conduct all the simulations at full scale.

Operating speed of the vessel is 6 ms^{-1}, but for two-phase simulations additionally a lower speed of 4 ms^{-1} was investigated.

The main analyzed quantity is the longitudinal velocity at the number of points, located in the propeller plane at different radii (see Fig. 2). The analysis was conducted both in single-phase and in two-phase formulations.

3.1 Single-phase simulation

At this stage of the study the ship motion with 6 ms^{-1} was considered at two different depth-to-draft ratios: H/T = 1.25 and 1.5. These conditions yield Fn_H = 1.2, 1.1, $Re = 8.1 \cdot 10^8$. Even though at such high Fn_H ship wavemaking is very intense and it can significantly influence the viscous wake of the ship, in the single-phase simulations the free surface was modeled by a symmetry plane. This is also done in the work of Raven [14], who studied the influence of shallow water on the frictional resistance.

The sizes of computational domain were $L_D = 9L_{wl}$, $H_D = \{1.25, 1.5\}T$, $B_D = 2L_{wl}$.

For the simulations the unstructured hex-dominant meshes, generated by StarCCM+® trimmer mesher were used. The approximate number of cells was 4M, the stern region was filled with isotropic uniform hexahedral cells with the edge size 0.06m. For full-scale simulations it is quite cumbersome to use low Reynolds meshes ($y^+ < 1$) therefore the wall

Variable	ship	inlet	outlet	bottom	river bank
p	$\frac{\partial p}{\partial n} = 0$	$\frac{\partial p}{\partial n} = 0$	$p = 0$	$\frac{\partial p}{\partial n} = 0$	$\frac{\partial p}{\partial n} = 0$
u	$u = 0$	$u = u_\infty$	$\frac{\partial u}{\partial n} = 0$	$u = u_\infty$	$u = u_\infty$
k	$\frac{\partial k}{\partial n} = 0$	$k = k_\infty$	$\frac{\partial k}{\partial n} = 0$	$\frac{\partial k}{\partial n} = 0$	$\frac{\partial k}{\partial n} = 0$
ω	$\omega = \omega_1(y^+)$	$\omega = \omega_\infty$	$\frac{\partial \omega}{\partial n} = 0$	$\omega = \omega_1(y^+)$	$\omega = \omega_1(y^+)$

Table 3: Boundary conditions for the single-phase simulations

functions were applied with $y^+ \approx 70$. Boundary conditions, imposed on the unknowns at the inlet, outlet, bottom, ship and river bank patches are summarized in the Table 3, where $\omega_\infty = 5U_\infty/L_D$, $k_\infty = 0.01\nu\omega_\infty$, $\omega_1(y^+) = \sqrt{\omega^2_{vis}(y^+) + \omega^2_{log}(y^+)}$ (see [15, 16] for details). Boundaries, corresponding to free surface and middle line plane were treated as symmetry planes. The simulation procedure was the following: first the RANS solution was obtained(`simpleFoam` solver), then it was used as an initial condition for URANS (for 10s) and after that the computation with the hybrid approach was conducted for the next 40s (`pimpleFoam` solver).

3.2 Two-phase simulation

Computations with the free surface were conducted for all the same geometry and conditions as for single-phase, except for the enlargement of the computational domain in the air region and additional consideration of speed $4ms^{-1}$. The boundary conditions for dynamic pressure, velocity and turbulent quantities were the same. For the volume fraction α Dirichlet boundary condition was imposed at the inlet (1 in the water region and 0 in the air region) and for all other boundaries $\frac{\partial \alpha}{\partial n} = 0$. The middle line plane was again considered as a symmetry plane. Summary of all computed cases can be found in the Table 1.

4 RESULTS AND DISCUSSION

4.1 Single-phase results

4.1.1 Analysis of the resolved kinetic energy

First of all, in order to make sure, that the mesh resolution was sufficient to resolve the turbulent motions in the wake, the ratio of resolved to modeled turbulence kinetic energy was analyzed (k_{res},k_{mod} respectively). As it is known, reliable results can be obtained only if $k_{res}/k_{mod} > 80\%$. For a hybrid simulation these quantities can be calculated as follows:

$$k_{mod} = \gamma k + (1 - \gamma)k_{sgs} \tag{10}$$

$$k_{res} = \frac{1}{2}\langle u_i' u_i' \rangle \tag{11}$$

$$k_{tot} = k_{res} + k_{tot} \tag{12}$$

The averaging in the formula (11) was done during the simulation (over 20 s.), k is the TKE from the hybrid model, k_{sgs} was estimated using the formula proposed by Mason and Callen [17]:

$$k_{sgs} = \frac{(C_s\Delta)^2|S|^2}{0.3} \tag{13}$$

Figure 4 shows the distribution of the analyzed ratio in the propeller plane for the case 1PH61. One can see, that at quite coarse resolution, used in the simulations, the percent of the resolved kinetic energy in the area of interest is already greater than 80. For other cases the similar result was obtained.

4.1.2 Vortical structures in the wake

In the Figure 5 the vortical structures identified in the wake using λ_2 criterion [18] are shown. One can easily see the difference between URANS and hybrid solutions. Both methods predict two stationary vortexes: at the skeg and the bilge. However, the scale resolving approach additionally shows flow instability, spreading downstream behind the skeg. Comparing different H/T ratios one can notice, that the amount of the eddies

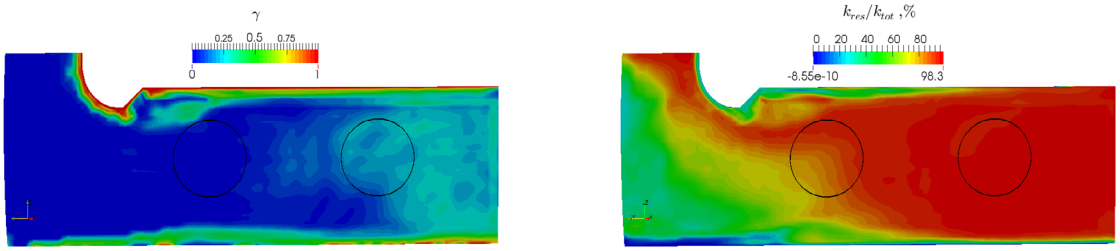

Figure 4: Average γ (left) and k_{res}/k_{tot} (right) in the propeller plane. Propeller disks are marked by black circles

depends on the fairway depth. Obviously the region filled with unsteady vortices becomes wider at lower depths. This can be easily explained by the fact, that the adverse pressure gradient grows, when H/T ratio decreases.

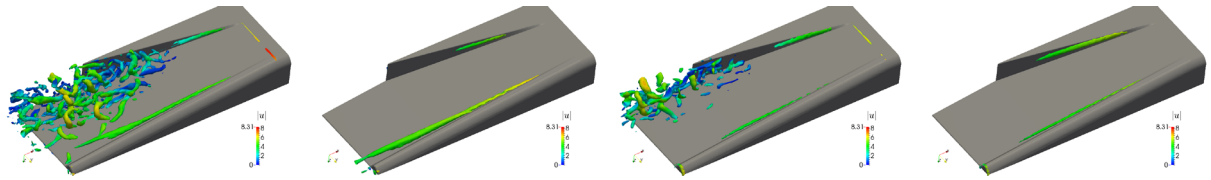

(a) (b) (c) (d)

Figure 5: Comparison of the vortex structures ($\lambda_2 = -15$) predicted by URANS and hybrid models in a single phase formulation: (a) - 1PH61, hybrid, (b) - 1PH61, URANS, (c) - 1PH62, hybrid, (d) - 1PH62, URANS. View of the stern area from below.

4.1.3 Longitudinal velocity oscillations

Figures 7(a-d) show the time history of velocity fluctuations at the points P1 and P2 (see Fig. 2), corresponding to $r/R = 0.8$ in the first(near the skeg) and second(near the bilge) propeller disks. The time interval [0;10] s corresponds to URANS solution. One can see that in both cases URANS method shows almost a steady velocity field. The fluctuations are negligibly small. After switching to the hybrid model the wake soon becomes unstable. It can be seen, that in general the fluctuation magnitude is much higher for the first propeller. Influence of the water depth on the vortical structures is also reflected in the

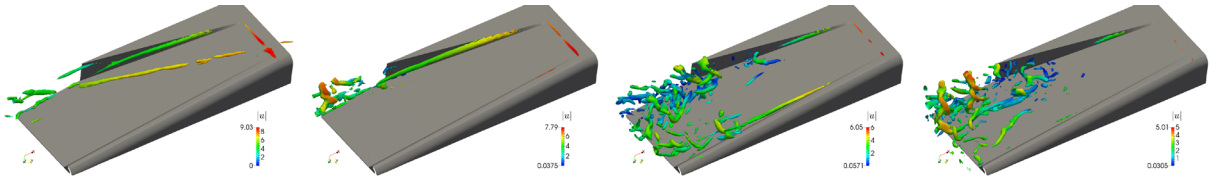

(a) (b) (c) (d)

Figure 6: Comparison of the vortex structures ($\lambda_2 = -15$) obtained from two-phase simulations with the hybrid model for different: (a) - 2PH61, (b) - 2PH62, (c) - 2PH41, (d) - 2PH42. View of the stern area from below.

Fig. 7(a-d). The maximum relative deviation from the mean value $\Delta u_x^{max} = \frac{max|u_x - \langle u_x \rangle|}{u_\infty}$ and the corrected sample standard deviation $s = \sqrt{\frac{1}{n-1}\sum_{i=0}^{n}(u_{x,i} - \langle u_x \rangle)^2}$ for both cases are shown in the Table 2. Although the flow for H/T=1.25 is richer with eddies, the maximum deviation of velocity from the mean value at considered points was observed for H/T=1.5, reaching 54% of the inflow velocity. Analysis of the power spectral density of the velocity fluctuations in the wake shows, that there are no dominant frequencies which could reveal the periodic processes. Inertial interval of the spectrum can be clearly seen and it follows the law of -5/3.

4.2 Two-phase results

The analysis of the two-phase flow at the same super-critical Fn_H (2PH61, 2PH62) showed the sharp change in the flow behaviour compared to single-phase. Namely, the fluctuations in the wake are almost vanished. The reason for this is the disappearance of the unsteady vortices (Fig. 6a,b). In order to understand the mechanism, that led to the oscillation suppression we have to look at the wave pattern in the stern (see Fig. 8). As mentioned above the flow in the stern area is similar to that of the 3D diffuser. However strong free surface deformation, usually observed in near-critical regime, causes in this case the change of the flow geometry. The phenomenon can be explained using the sketch presented in Fig.9). First, the fluid motion follows the free surface contour, resulting in the appearance of negative vertical velocities in the area in front and behind the ship bottom edge. Second, the step of the diffuser gets smaller. Due to this effect and

water level depression the positive pressure gradient along the hull in the stern decreases. For these reasons the reduction of both separation and formation of strong vortices is observed. To check that the captured phenomenon is physically adequate and is caused by free surface deformation, the computations with subcritical $Fn_H < 1$ were conducted, at the speed of $4ms^{-1}$ (cases 2PH41, 2PH42). The pictures of the stern wave patterns and the comparison of the corresponding unsteady vortical structures for different two-phase cases are presented in the Fig. 6,8. The decrease of Fr_H expectedly diminished the stern wave, making the flow geometry closer to that in single-phase simulation. Because of this

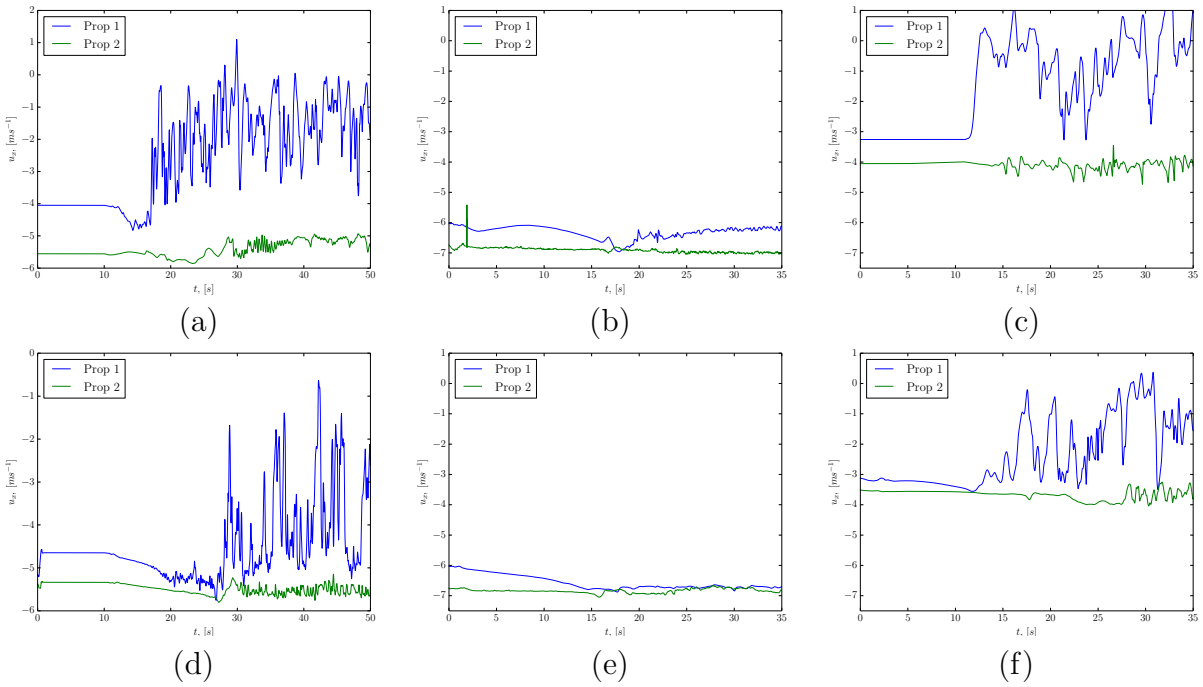

Figure 7: Time history of longitudinal velocity at two points in propeller disks. (a) - 1PH61, (b) - 2PH61, (c) - 2PH41, (d) - 1PH62, (e) - 2PH62, (f) - 2PH42

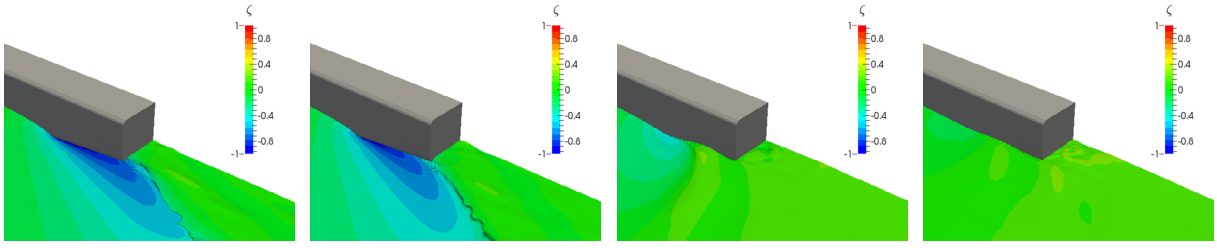

Figure 8: Stern wave pattern for different cases.(a) - 2PH61, (b) - 2PH62 , (c) - 2PH41, (d) - 2PH42

the separation behind the skeg appeared again and thus the flow behaviour is very similar to that seen in one-phase case. This confirms, that the wavemaking directly influences the wake unsteadiness. To authors' knowledge this effect has not been discussed in literature so far. It should be mentioned, that even though in the critical regime the separation is suppressed and cannot influence the loadings on the first propeller, the observed change of the water level causes the aeration of the second propeller, potentially leading to another problems.

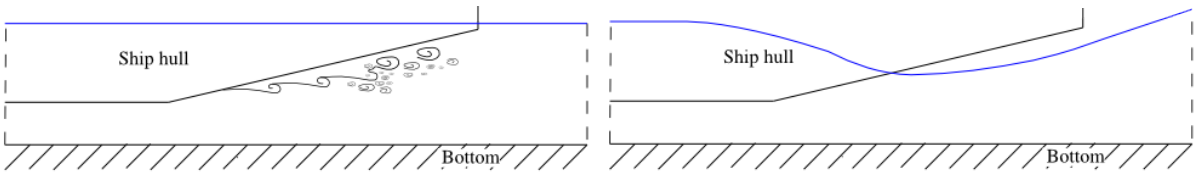

Figure 9: Schematic explanation of the free surface influence on the wake unsteadiness: left - flow geometry in one-phase simulation , right - the case of critical Fr_H, stern wave causes the change of flow geometry

5 CONCLUSIONS

The main conclusion that can be drawn from the presented results is the strong dependence of the unsteady effects in the wake on the waterway depth and the operating speed of the vessel. Even though the intensity of the observed velocity fluctuations is assumed to be much higher than that in real conditions, since the suction force of the propellers was not accounted for, the flow instabilities may well considerably influence the propeller loadings. The evaluation of the influence of suction force as well as other factors like drift angle will be performed in the further research.

REFERENCES

[1] N. Kornev, A. Taranov, E. Shchukin, and L. Kleinsorge. Development of hybrid URANS-LES methods for flow simulation in the ship stern area. *Ocean Engineering*, 38:1831–1838, 2011.

[2] B. Barras. *Ship design and performance for masters and mates.* Butterworth-Heinemann, 2004.

[3] Nikolai Kornev. *Propellertheorie.* Shaker, 2009.

[4] Larsson L., Stern F., and M. Visonneau. Gothenburg 2010—a workshop on numerical ship hydrodynamics. In *Proceedings. vol. 2.* Department of Naval Architecture and Ocean Engineering, Chalmers University of Technology, 2010.

[5] J. Binns, R. Brown, and N. Bose. Proceedings Of The Third International Symposium on Marine Propulsors. Australian Maritime College, University of Tasmania, 2013.

[6] J. Fröhlich and D. von Terzi. Hybrid LES/RANS Methods for the Simulation of Turbulent Flows. *Progress in Aerospace Sciences*, 44:349–377, 2008.

[7] S.B. Pope. *Turbulent Flows*. Cambridge University Press, 2000.

[8] P. Sagaut, S. Deck, and M. Terracol. *Multiscale and Multiresolution Approaches in Turbulence: LES, DES and Hybrid RANS/LES Methods : Applications and Guidelines*. Imperial College Press, 2013.

[9] D. K. Lilly. A proposed modification of the Germano subgridscale closure method. *Physics of Fluids A: Fluid Dynamics (1989-1993)*, 4(3):633–635, 1992.

[10] F. R Menter, M. Kuntz, and R. Langtry. Ten Years of Industrial Experience with the SST Turbulence Model. In K. Hanjalic, Y. Nagano, and M. Tummers, editors, *Turbulence, Heat and Mass Transfer 4*. Begell House, Inc., 2003.

[11] H. Schlichting. *Boundary layer theory*. Springer, 2000.

[12] N. Kornev, A. Taranov, E. Shchukin, J. Springer, M. Palm, and Yu. Batrak. Development, application and validation of hybrid URANS-LES methods for flow simulation in the ship stern area. In *29th Symposium on Naval Hydrodynamics, Gothenburg, Sweden*, 2012.

[13] S.M. Damian. *An Extended Mixture Model for the Simultaneous Treatment of Short and Long Scale Interface*. Universidad Nacional del Litoral, Santa Fe, Argentina, 2013.

[14] Hoyte C. Raven. A computational study of shallow-water effects on ship viscous resistance. In *Proceedings of 29th Symposium on Naval Hydrodynamics*, 2012.

[15] Florian R Menter. Two-equation eddy-viscosity turbulence models for engineering applications. *AIAA journal*, 32(8):1598–1605, 1994.

[16] Florian Menter, J Carregal Ferreira, Thomas Esch, Brad Konno, and AC Germany. The SST turbulence model with improved wall treatment for heat transfer predictions in gas turbines. In *Proceedings of the international gas turbine congress*, pages 2–7, 2003.

[17] P. J. Mason and N. S. Callen. On the magnitude of the subgrid-scale eddy coefficient in large-eddy simulations of turbulent channel flow. *Journal of Fluid Mechanics*, 162:439–462, 1 1986.

[18] J. Jeong and F. Hussain. On the identification of a vortex. *Journal of Fluid mechanics*, 285:69–94, 1995.